INTERNATIONAL JOURNAL FOR NUMERICAL METHODS IN FLUIDS
Int. J. Numer. Meth. Fluids 2008; **57**:1485–1504
Published online 13 November 2007 in Wiley InterScience (www.interscience.wiley.com). DOI: 10.1002/fld.1667

Continuous and discrete adjoint approaches for aerodynamic shape optimization with low Mach number preconditioning

V. G. Asouti, A. S. Zymaris, D. I. Papadimitriou and K. C. Giannakoglou*, †, ‡

Laboratory of Thermal Turbomachines, Department of Mechanical Engineering, Parallel CFD and Optimization Unit, National Technical University of Athens, Athens, Greece

SUMMARY

Discrete and continuous adjoint approaches for use in aerodynamic shape optimization problems at all flow speeds are developed and assessed. They are based on the Navier–Stokes equations with low Mach number preconditioning. By alleviating the large disparity between acoustic waves and fluid speeds, the preconditioned flow and adjoint equations are numerically solved with affordable CPU cost, even at the so-called incompressible flow conditions. Either by employing the adjoint to the preconditioned flow equations or by preconditioning the adjoint to the 'standard' flow equations (under certain conditions the two formulations become equivalent, as proved in this paper), efficient optimization methods with reasonable cost per optimization cycle, even at very low Mach numbers, are derived. During the mathematical development, a couple of assumptions are made which are proved to be harmless to the accuracy in the computed gradients and the effectiveness of the optimization method. The proposed approaches are validated in inviscid and viscous flows in external aerodynamics and turbomachinery flows at various Mach numbers. Copyright © 2007 John Wiley & Sons, Ltd.

Received 11 July 2007; Revised 2 October 2007; Accepted 8 October 2007

KEY WORDS: aerodynamic shape optimization; adjoint approach; low Mach number preconditioning

1. INTRODUCTION

During the last years, significant progress has been made in the use of adjoint codes in aerodynamic shape optimization problems. Working with deterministic optimization methods, the ability to

*Correspondence to: K. C. Giannakoglou, Laboratory of Thermal Turbomachines, Department of Mechanical Engineering, Parallel CFD and Optimization Unit, National Technical University of Athens, P.O. Box 64069, 15710 Athens, Greece.
†E-mail: kgianna@central.ntua.gr
‡Associate Professor.

Contract/grant sponsor: NTUA Basic Research Program 'Lefkippos'
Contract/grant sponsor: State Scholarships Foundation of Greece

efficiently compute the gradient of an objective function F with respect to the design variables is crucial. In view of the above, the main advantage of the adjoint technique is that it computes the sensitivity derivatives of F at the cost of an 'equivalent' flow solution, irrespective of the number of design variables. This cost is quite low, compared with that of other methods, such as finite differences or the complex variable technique [1]. When the gradients are available, methods such as steepest descent, conjugate gradient or quasi-Newton can be used. Two adjoint approaches, the continuous and the discrete one, can be found in the literature. In the continuous approach, the adjoint partial differential equations are first derived from the flow ones and, then, discretized and numerically solved. In the discrete approach, the discrete adjoint equations are derived directly from the discretized flow equations. A detailed comparison of the two approaches can be found in [2].

In fluid mechanics, the adjoint method was introduced by Pironneau [3] for potential flows, although Jameson was the first to use the continuous adjoint method with hyperbolic flow equations [4, 5]. Since then, the progress in the use of adjoint techniques in the field of aerodynamics was significant; several groups have developed adjoint codes based on either the continuous [4, 6, 7] or the discrete approach [8, 9], using the Euler or the Navier–Stokes equations as state equations. Nowadays, the use of adjoint approaches is extended to the design of complete aircraft configurations [10–12]. In turbulent flows, the introduction of additional adjoint equations that are dual to the turbulence model equations has been proposed in [9, 13]; however, many well-performing adjoint methods ignore these extra equations. Apart from shape reconstruction problems based on a given pressure distribution over the shape contour, other objective functions dealing with drag minimization and/or lift maximization, shock wave reduction in external aerodynamics [14, 15], losses minimization in cascades [16], etc. are in use. Adjoint formulations for unsteady aerodynamic design have been presented in [17, 18]. To further reduce the optimization CPU cost, instead of separately solving the flow and adjoint equations along with the equation to update the design variables, all three of them can simultaneously be solved, through the so-called one-shot method [19–21]. A different approach which, under circumstances, may lower the total computational cost is the incomplete gradient method [22, 23], whereby terms of minor importance in the gradient expression are omitted. By doing so, the sensitivity derivatives become less accurate although the method usually becomes more efficient.

All adjoint formulations in the literature have been derived starting from the non-preconditioned Navier–Stokes equations; hence, the numerical solution of both the flow and adjoint equations suffers from excessive CPU cost when low-speed designs are carried out. Hence, in this case, an optimization algorithm based on the corresponding non-preconditioned adjoint method performs badly. It is known that the main reason for the performance degradation of time-marching compressible flow solvers at low speeds is the large disparity between acoustic waves and fluid speeds in both the flow and adjoint equations. Hence, during the optimization cycle, the observed degradation in convergence speed at low flow speeds is associated with both the numerical solution of the flow equations and that of the adjoint equations. As a remedy to this problem, Turkel [24] proposed the use of preconditioned flow equations, formed by multiplying their pseudo-time derivative by the preconditioning matrix. Dealing with steady flows, preconditioning by no means affects the steady-state solution of the flow equations. Various preconditioning matrices for the flow equations have been proposed [24–26]. They are all defined in terms of the local Mach number and degenerate to the unit matrix at sonic speed. The expected gain from the use of low Mach number preconditioned compressible fluid flow codes becomes noticeable at very low flow speeds, practically at the so-called incompressible flow regime.

DOI: 10.1002/fld

Considering the aforementioned convergence speed degradation, an adjoint formulation for the preconditioned Navier–Stokes equations is proposed. Our aim is to develop a system of adjoint equations that are dual to the preconditioned flow equations and, hence, converge satisfactorily even at low flow speeds. The theoretical development is presented for both discrete and continuous approaches. The continuous adjoint is based on the formulation proposed in [27] for the non-preconditioned Navier–Stokes equations. As in [27], the resulting expression for the gradient of the objective function is free of field integrals of variations in nodal coordinates, i.e. field variations in grid metrics.

2. PRECONDITIONED NAVIER–STOKES EQUATIONS

2.1. Formulation

The Navier–Stokes equations are expressed in the conservative form as

$$\frac{\partial \mathbf{U}}{\partial t}+\frac{\partial \mathbf{f}_i^{\text{inv}}}{\partial x_i}-\frac{\partial \mathbf{f}_i^{\text{vis}}}{\partial x_i}=0 \tag{1}$$

where $\mathbf{U}=[\varrho, \varrho\mathbf{u}, E]^{\mathrm{T}}$ is the vector of conservative variables. The inviscid and viscous fluxes are given by

$$\mathbf{f}_i^{\text{inv}}=\begin{bmatrix} \rho u_i \\ \rho u_i \mathbf{u}+p\boldsymbol{\delta}_i \\ u_i(E+p) \end{bmatrix}, \quad \mathbf{f}_i^{\text{vis}}=\begin{bmatrix} 0 \\ \boldsymbol{\tau}_i \\ u_j\tau_{ij}+q_i \end{bmatrix} \tag{2}$$

where $\mathbf{u}$ is the velocity vector, $\boldsymbol{\tau}_i=[\tau_{i1}, \tau_{i2}]^{\mathrm{T}}$ are the viscous stresses, $\boldsymbol{\delta}_i=[\delta_{i1}, \delta_{i2}]^{\mathrm{T}}$ are the Kronecker symbols and $q_i=k\partial T/\partial x_i$ are the thermal flux components. The low Mach preconditioned Navier–Stokes equations are derived from Equation (1) by multiplying the pseudotime-step term by the inverse of the preconditioning matrix Γ. Hence

$$\frac{\partial \mathbf{U}}{\partial t}+\Gamma\left(\frac{\partial \mathbf{f}_i^{\text{inv}}}{\partial x_i}-\frac{\partial \mathbf{f}_i^{\text{vis}}}{\partial x_i}\right)=0 \tag{3}$$

Γ is given by [25]

$$\Gamma=\left(\frac{\partial \mathbf{U}}{\partial \mathbf{V}}\right)\begin{bmatrix} 1 & 0 & 0 & -\dfrac{1-a}{c^2} \\ 0 & 1 & 0 & 0 \\ 0 & 0 & 1 & 0 \\ 0 & 0 & 0 & a \end{bmatrix}\left(\frac{\partial \mathbf{U}}{\partial \mathbf{V}}\right)^{-1} \tag{4}$$

where $\mathbf{V}=[\varrho, \mathbf{u}, p]^{\mathrm{T}}$ is the vector of non-conservative variables, $(\partial\mathbf{U}/\partial\mathbf{V})$ is the transformation matrix from the non-conservative to the conservative variables and $a=\min(1, M^2)$, where M is the local Mach number. Hence, the inviscid part of the preconditioned Navier–Stokes equations

DOI: 10.1002/fld

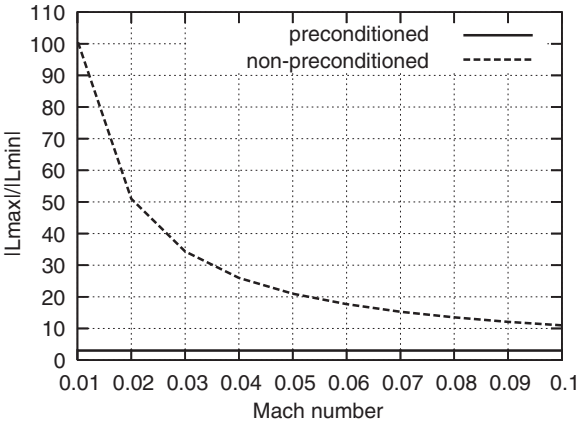

Figure 1. Comparison of the condition number ($|\lambda_{\max}|/|\lambda_{\min}|$) of the preconditioned and non-preconditioned systems in the range $0.01 \leqslant M \leqslant 0.1$.

is expressed as

$$\frac{\partial \mathbf{U}}{\partial t} + A_{\Gamma_x} \frac{\partial \mathbf{U}}{\partial x} + A_{\Gamma_y} \frac{\partial \mathbf{U}}{\partial y} = 0 \tag{5}$$

where $A_{\Gamma_x} = \Gamma A_x$ and $A_{\Gamma_y} = \Gamma A_y$ are the preconditioned Jacobians. Their eigenvalues

$$\lambda_1 = \lambda_2 = \mathbf{u} \cdot \mathbf{n}, \quad \lambda_{3,4} = \frac{1}{2} \left\{ (1+a)\mathbf{u} \cdot \mathbf{n} \pm \sqrt{[(1-a)\mathbf{u} \cdot \mathbf{n}]^2 + 4ac^2 |\mathbf{n}|^2} \right\} \tag{6}$$

are much more clustered than those of the non-preconditioned system ($\lambda_1^* = \lambda_2^* = \mathbf{u} \cdot \mathbf{n}$, $\lambda_{3,4}^* = \mathbf{u} \cdot \mathbf{n} \pm c|\mathbf{n}|$) ensuring, thus, better convergence properties. Figure 1 compares the ratio $|\lambda_{\max}|/|\lambda_{\min}|$ (condition number) of the two systems. As the Mach number approaches zero, the condition number of the non-preconditioned equations increases, leading to an ill-conditioned system with slow convergence characteristics; in contrast, the condition number of the preconditioned system remains close to unit.

2.2. Discretization and numerical solution

The finite-volume technique with a second-order upwind scheme for the inviscid fluxes is used for the solution of the flow equations on unstructured grids with triangular elements. At each grid node P, the corresponding finite volume Ω_P is defined by connecting the barycentres of the surrounding triangles and the mid-points of the edges emanating from P (Figure 2). Along its boundary $\partial\Omega_P$, the outward normal vector is denoted by $\mathbf{n} = (n_x, n_y)$. By integrating Equations (3) over the finite volume of node P, we obtain

$$\frac{\Omega_P}{\Delta t_P} \Delta \mathbf{U}_P + \Gamma_P \sum_{Q \in \mathrm{nei}(P)} \mathbf{\Phi}_{PQ} = 0 \tag{7}$$

DOI: 10.1002/fld

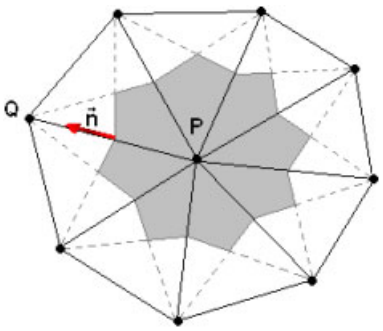

Figure 2. Control volume surrounding a node of an unstructured grid with triangular elements.

where $\mathbf{\Phi}_{PQ}$ is the numerical flux ($\mathbf{f}_i n_i$) associated with the part of $\partial\Omega_P$ which is the interface of the finite volumes of P and Q. Equation (7) is expressed as

$$\frac{\Omega_P}{\Delta t_P}\Delta\mathbf{U}_P + \mathbf{R}_P^{\Gamma} = 0 \tag{8}$$

where $\mathbf{R}_P^{\Gamma} = \Gamma_P \mathbf{R}_P$ and

$$\mathbf{R}_P = \sum_{Q\in \mathrm{nei}(P)} \mathbf{\Phi}_{PQ}^{\mathrm{inv}} - \sum_{T\in \mathrm{nei}_T(P)} \mathbf{\Phi}_{P,T}^{\mathrm{vis}} \tag{9}$$

where $\mathrm{nei}(P)$ denotes the set of the neighbouring nodes linked to P by a grid edge and $\mathrm{nei}_T(P)$ is the set of triangles surrounding P. Equation (9) is compatible with an edge-based discretization scheme for the convection terms and an element-based scheme for the viscous ones.

A 1D Roe approximate Riemann solver [28] is used to compute the inviscid fluxes $\mathbf{\Phi}_{PQ}^{\mathrm{inv}}$ and second-order accuracy is obtained through variables' extrapolation. Hence, for the preconditioned flow equations, according to van Leer *et al.* [29], the inviscid numerical flux can be expressed as

$$\begin{aligned}\mathbf{\Phi}_{PQ}^{\mathrm{inv}} &= \tfrac{1}{2}[A_P\mathbf{U}_P + A_Q\mathbf{U}_Q] - \tfrac{1}{2}\Gamma^{-1}\Gamma|\tilde{A}_{PQ}|\Delta\mathbf{U}_{PQ} \\ &\simeq \tfrac{1}{2}[A_P\mathbf{U}_P + A_Q\mathbf{U}_Q] - \tfrac{1}{2}\tilde{\Gamma}_{PQ}^{-1}|\tilde{A}_{\Gamma_{PQ}}|\Delta\mathbf{U}_{PQ}\end{aligned} \tag{10}$$

where $A_i = \partial\mathbf{f}_i/\partial\mathbf{U}$, $A_P = A_{i_P} n_{PQ,i}$, $A_Q = A_{i_Q} n_{PQ,i}$, whereas $|\tilde{A}_{PQ}|$ is the Roe-averaged Jacobian at the midnode and $\Delta\mathbf{U}_{PQ} = \mathbf{U}_Q - \mathbf{U}_P$. The viscous fluxes are computed by assuming linearly distributed primitive flow variables $\mathbf{V}$ over each triangular element. To deal with turbulent flows, the Spalart–Allmaras [30] turbulence model is used. The numerical solution of the discretized preconditioned flow equations is carried out using the point-implicit Jacobi method.

DOI: 10.1002/fld

3. ADJOINT FORMULATION BASED ON THE PRECONDITIONED FLOW EQUATIONS

3.1. Objective functions

The inverse design of isolated or cascade airfoils that reproduce a desired pressure distribution $p_{\text{tar}}(s)$ over the solid walls S_{w} can be associated with the minimization of the objective function

$$F=\frac{1}{2}\int_{S_{\text{w}}}(p-p_{\text{tar}})^2\,\mathrm{d}S \tag{11}$$

The variation in F due to any variation in the design variables $\mathbf{b}$ is

$$\delta F=\int_{S_{\text{w}}}(p-p_{\text{tar}})\delta p\,\mathrm{d}S+\frac{1}{2}\int_{S_{\text{w}}}(p-p_{\text{tar}})^2\delta(\mathrm{d}S) \tag{12}$$

where $\delta(\mathrm{d}S)=\phi_1(\delta\mathbf{b})$ depends on the parameterization.

On the other hand, the design of an airfoil with minimum drag (c_{d}) and given lift coefficient ($c_{\text{l}}=c_{\text{l}_{\text{tar}}}$) can be based on the following objective function:

$$F=(c_{\text{l}}-c_{\text{l}_{\text{tar}}})^2+\beta c_{\text{d}}^2 \tag{13}$$

where β scales the relative significance of lift and drag. The variation in F is given by

$$\delta F=2(c_{\text{l}}-c_{\text{l}_{\text{tar}}})\delta c_{\text{l}}+2\beta c_{\text{d}}\delta c_{\text{d}} \tag{14}$$

with

$$\begin{aligned} c_{\text{d,l}} &= \frac{1}{\varpi}\int p(q_1\cos a+q_2\sin a)\,\mathrm{d}S \\ \delta c_{\text{d,l}} &= \frac{1}{\varpi}\int \delta p(q_1\cos a+q_2\sin a)\,\mathrm{d}S+\frac{1}{\varpi}\int p\cos a\,\delta(q_1\,\mathrm{d}S)+\frac{1}{\varpi}\int p\sin a\,\delta(q_2\,\mathrm{d}S) \end{aligned} \tag{15}$$

where $(q_1,q_2)=(n_1,n_2)$ for c_{d} or $(q_1,q_2)=(t_1,t_2)$ for c_{l}, $\mathbf{t}=(t_1,t_2)=(n_2,-n_1)$ is the tangent vector, a is the infinite flow angle, ϖ is the usual denominator used in the definition of c_{l} and c_{d} ($\varpi=\frac{1}{2}\varrho|\mathbf{u}|^2C$, where C is the chord) and $\delta(q_i\,\mathrm{d}S)=\phi_2(\delta\mathbf{b})$ depends on the parameterization of the shape. Equation (15) was written for inviscid flows, although its viscous counterpart (including viscous stresses) will be used in the Results section.

3.2. Continuous adjoint formulation using preconditioning

In this section, the continuous adjoint method for the inverse design of aerodynamic shapes at low Mach number flows, based on the preconditioned Navier–Stokes equations as state equations, is presented. The variation in the augmented objective function is expressed as

$$\delta F_{\text{aug}}=\delta F+\int_{\Omega}\boldsymbol{\Psi}^{\text{T}}\delta\left[\Gamma\left(\frac{\partial\mathbf{f}_i}{\partial x_i}\right)\right]\mathrm{d}\Omega=\delta F+\int_{\Omega}\boldsymbol{\Psi}^{\text{T}}\Gamma\delta\left(\frac{\partial\mathbf{f}_i}{\partial x_i}\right)\mathrm{d}\Omega \tag{16}$$

DOI: 10.1002/fld

where $\mathbf{f}_i = \mathbf{f}_i^{\text{inv}} - \mathbf{f}_i^{\text{vis}}$. Note that no assumption about $\delta\Gamma$ is made since $\partial \mathbf{f}_i / \partial x_i = 0$. From a different viewpoint, one may consider the last integrand in Equation (16) to be the product of the adjoint vector $\boldsymbol{\Psi}$ and the variation in the flow equations multiplied by Γ; both considerations lead to the same expression. As proved in [27], the variation in the gradient of any quantity Φ is expressed in terms of the gradient of $\delta\Phi$ and the variations in nodal coordinates, namely

$$\delta\left(\frac{\partial \Phi}{\partial x_i}\right) = \frac{\partial(\delta\Phi)}{\partial x_i} - \frac{\partial \Phi}{\partial x_k}\frac{\partial(\delta x_k)}{\partial x_i} \tag{17}$$

Consequently,

$$\int_\Omega \boldsymbol{\Psi}_\Gamma^{\mathrm{T}} \delta\left(\frac{\partial \mathbf{f}_i}{\partial x_i}\right) \mathrm{d}\Omega = \int_\Omega \boldsymbol{\Psi}_\Gamma^{\mathrm{T}} \frac{\partial(\delta \mathbf{f}_i)}{\partial x_i}\,\mathrm{d}\Omega - \int_\Omega \boldsymbol{\Psi}_\Gamma^{\mathrm{T}} \frac{\partial \mathbf{f}_i}{\partial x_k}\frac{\partial(\delta x_k)}{\partial x_i}\,\mathrm{d}\Omega \tag{18}$$

where $\boldsymbol{\Psi}_\Gamma = \Gamma^{\mathrm{T}} \boldsymbol{\Psi}$ will be referred to as the vector of preconditioned adjoint variables. It is a matter of integration by parts to obtain

$$\begin{aligned}\int_\Omega \boldsymbol{\Psi}_\Gamma^{\mathrm{T}} \delta\left(\frac{\partial \mathbf{f}_i}{\partial x_i}\right) \mathrm{d}\Omega = &- \int_\Omega \delta \mathbf{f}_i^{\mathrm{T}} \frac{\partial \boldsymbol{\Psi}_\Gamma}{\partial x_i}\,\mathrm{d}\Omega + \int_{S_{\mathrm{i,o,w}}} \boldsymbol{\Psi}_\Gamma^{\mathrm{T}} \delta \mathbf{f}_i n_i\,\mathrm{d}S \\ &+ \int_\Omega \frac{\partial}{\partial x_i}\left(\boldsymbol{\Psi}_\Gamma^{\mathrm{T}} \frac{\partial \mathbf{f}_i}{\partial x_k}\right)\delta x_k\,\mathrm{d}\Omega - \int_{S_{\mathrm{w}}} \boldsymbol{\Psi}_\Gamma^{\mathrm{T}} \frac{\partial \mathbf{f}_i}{\partial x_k}\delta x_k n_i\,\mathrm{d}S\end{aligned} \tag{19}$$

where S_{i}, S_{o} and S_{w} are the inlet, outlet and wall boundaries, respectively. The last integral is defined only along the parameterized solid walls, where $\delta x_k \neq 0$. We further develop Equation (19) separately for the inviscid and viscous terms. For the inviscid terms in Equation (19), we obtain

$$\begin{aligned}\int_\Omega \boldsymbol{\Psi}_\Gamma^{\mathrm{T}} \delta\left(\frac{\partial \mathbf{f}_i^{\text{inv}}}{\partial x_i}\right) \mathrm{d}\Omega = &- \int_\Omega \delta \mathbf{f}_i^{\text{inv}T} \frac{\partial \boldsymbol{\Psi}_\Gamma}{\partial x_i}\,\mathrm{d}\Omega + \int_{S_{\mathrm{i,o}}} \delta \mathbf{U}^{\mathrm{T}} (A_n^{\mathrm{T}} \boldsymbol{\Psi}_\Gamma)\,\mathrm{d}S \\ &+ \int_{S_{\mathrm{w}}} \Psi_{\Gamma,i+1} n_i \delta p\,\mathrm{d}S + \int_{S_{\mathrm{w}}} [\Psi_{\Gamma,i+1} p - \boldsymbol{\Psi}_\Gamma^{\mathrm{T}} \mathbf{f}_i^{\text{inv}}]\delta(n_i\,\mathrm{d}S) \\ &+ \int_\Omega \frac{\partial \mathbf{U}^{\mathrm{T}}}{\partial x_k} A_i^{\mathrm{T}} \frac{\partial \boldsymbol{\Psi}_\Gamma}{\partial x_i}\delta x_k\,\mathrm{d}\Omega - \int_{S_{\mathrm{w}}} \frac{\partial \mathbf{U}^{\mathrm{T}}}{\partial x_k} A_n^{\mathrm{T}} \boldsymbol{\Psi}_\Gamma \delta x_k\,\mathrm{d}S\end{aligned} \tag{20}$$

In case of viscous flows, two assumptions are made; the bulk viscosity is assumed to be independent of the temperature and, for turbulent flows, the variation in the turbulent viscosity coefficient is not taken into account. Hence

$$\begin{aligned}-\int_\Omega \boldsymbol{\Psi}_\Gamma^{\mathrm{T}} \delta\left(\frac{\partial \mathbf{f}_i^{\text{vis}}}{\partial x_i}\right) \mathrm{d}\Omega = &\int_\Omega \delta \mathbf{f}_i^{\text{vis}\,\mathrm{T}} \frac{\partial \boldsymbol{\Psi}_\Gamma}{\partial x_i}\,\mathrm{d}\Omega - \int_{S_{\mathrm{i,o,w}}} \boldsymbol{\Psi}_\Gamma^{\mathrm{T}} \delta \mathbf{f}_i^{\text{vis}} n_i\,\mathrm{d}S \\ &- \int_\Omega \frac{\partial}{\partial x_i}\left(\boldsymbol{\Psi}_\Gamma^{\mathrm{T}} \frac{\partial \mathbf{f}_i^{\text{vis}}}{\partial x_k}\right)\delta x_k\,\mathrm{d}\Omega + \int_{S_{\mathrm{w}}} \boldsymbol{\Psi}_\Gamma^{\mathrm{T}} \frac{\partial \mathbf{f}_i^{\text{vis}}}{\partial x_k}\delta x_k n_i\,\mathrm{d}S\end{aligned} \tag{21}$$

DOI: 10.1002/fld

For the viscous fluxes, we obtain

$$\int_\Omega \delta \mathbf{f}_i^{\mathrm{vis\,T}} \frac{\partial \boldsymbol{\Psi}_\Gamma}{\partial x_i}\,\mathrm{d}\Omega = \int_\Omega \delta\tau_{ij}\left(\frac{\partial \Psi_{\Gamma_{j+1}}}{\partial x_i} + u_j \frac{\partial \Psi_{\Gamma_4}}{\partial x_i}\right)\mathrm{d}\Omega + \int_\Omega \delta u_i \tau_{ij} \frac{\partial \Psi_{\Gamma_4}}{\partial x_i}\,\mathrm{d}\Omega + \int_\Omega \delta q_i \frac{\partial \Psi_{\Gamma_4}}{\partial x_i}\,\mathrm{d}\Omega \tag{22}$$

where the variation in stresses $\delta\tau_{ij}$ reads

$$\delta\tau_{ij} = \mu\left[\left(\frac{\partial(\delta u_i)}{\partial x_j} + \frac{\partial(\delta u_j)}{\partial x_i}\right) - \frac{2}{3}\delta_{ij}\frac{\partial(\delta u_k)}{\partial x_k}\right] - \mu\left[\left(\frac{\partial u_i}{\partial x_k}\frac{\partial(\delta x_k)}{\partial x_j} + \frac{\partial u_j}{\partial x_k}\frac{\partial(\delta x_k)}{\partial x_i}\right) - \frac{2}{3}\delta_{ij}\frac{\partial u_l}{\partial x_k}\frac{\partial(\delta x_k)}{\partial x_l}\right] \tag{23}$$

The thermal flux variation term is expressed as

$$\int_\Omega \delta q_i \frac{\partial \Psi_{\Gamma_4}}{\partial x_i}\,\mathrm{d}\Omega = \int_\Omega k\left(\frac{\partial(\delta T)}{\partial x_i} - \frac{\partial T}{\partial x_k}\frac{\partial(\delta x_k)}{\partial x_i}\right)\frac{\partial \Psi_{\Gamma_4}}{\partial x_i}\,\mathrm{d}\Omega \tag{24}$$

where k is the coefficient of thermal conductivity. The first surface integral in Equation (21) is further analysed as follows:

$$-\int_{S_{\mathrm{i,o,w}}} \boldsymbol{\Psi}_\Gamma \delta \mathbf{f}_i^{\mathrm{vis\,T}} n_i\,\mathrm{d}S = -\int_{S_\mathrm{w}} [(\Psi_{\Gamma_{i+1}} + u_i \Psi_{\Gamma_4})\delta\tau_{ij} + \Psi_{\Gamma_4}\tau_{ij}\delta u_i + \Psi_{\Gamma_4}\delta q_j] n_j\,\mathrm{d}S \tag{25}$$

where all terms in Equation (25) containing velocities or their variations can be eliminated (no-slip condition). Equations (16) and (18)–(25) produce the final expression for δF_{aug} which is

$$\begin{aligned}\delta F_{\mathrm{aug}} = \delta F &- \int_\Omega \left(\delta\mathbf{U} - \frac{\partial \mathbf{U}}{\partial x_k}\delta x_k\right)^{\mathrm{T}}\left(A_i^{\mathrm{T}}\frac{\partial \boldsymbol{\Psi}_\Gamma}{\partial x_i}\right)\mathrm{d}\Omega - \int_\Omega \left(\delta\mathbf{V} - \frac{\partial \mathbf{V}}{\partial x_k}\delta x_k\right)^{\mathrm{T}}\mathbf{K}\,\mathrm{d}\Omega \\ &- \int_{S_\mathrm{w}} \frac{\partial \mathbf{U}^{\mathrm{T}}}{\partial x_k} A_n{}^{\mathrm{T}} \boldsymbol{\Psi}_\Gamma \delta x_k\,\mathrm{d}S + \int_{S_\mathrm{w}} \Psi_{\Gamma_{i+1}} n_i \delta p\,\mathrm{d}S + \int_{S_\mathrm{w}} [\Psi_{\Gamma_{i+1}} p - \boldsymbol{\Psi}_\Gamma^{\mathrm{T}} \mathbf{f}_i^{\mathrm{inv}}]\delta(n_i\,\mathrm{d}S) \\ &+ \int_{S_{\mathrm{i,o}}} \delta\mathbf{U}^{\mathrm{T}}(A_n^{\mathrm{T}}\boldsymbol{\Psi}_\Gamma)\,\mathrm{d}S + \int_{S_\mathrm{w}} k\delta T \frac{\partial \Psi_{\Gamma_4}}{\partial x_i} n_i\,\mathrm{d}S - \int_{S_\mathrm{w}} \Psi_{\Gamma_4}\delta(q_j n_j\,\mathrm{d}S) \\ &+ \int_{S_\mathrm{w}} \Psi_{\Gamma_4} q_j \delta(n_j\,\mathrm{d}S) - \int_{S_\mathrm{w}} \frac{\partial u_i}{\partial x_k}\tau_{ij}^{(\Psi_\Gamma)}\delta x_k n_j\,\mathrm{d}S + \int_{S_\mathrm{w}} \frac{\Psi_{\Gamma_{i+1}}}{n_i}\tau_{ij}\delta(n_i n_j)\,\mathrm{d}S \\ &- \int_{S_\mathrm{w}} k\frac{\partial T}{\partial x_k}\frac{\partial \Psi_{\Gamma_4}}{\partial x_i}\delta x_k n_i\,\mathrm{d}S + \int_{S_\mathrm{w}} \boldsymbol{\Psi}_\Gamma \frac{\partial \mathbf{f}_i^{\mathrm{vis}}}{\partial x_k}\delta x_k n_i\,\mathrm{d}S\end{aligned} \tag{26}$$

DOI: 10.1002/fld

In Equation (26), the elimination of field integrals expressed in terms of $\partial\mathbf{U}/\partial\mathbf{b}=\delta\mathbf{U}-\partial\mathbf{U}/\partial x_k\delta x_k$ requires the satisfaction of the field preconditioned adjoint equations

$$\frac{\partial\boldsymbol{\Psi}}{\partial t}-A_i^{\mathrm{T}}\frac{\partial(\Gamma^{\mathrm{T}}\boldsymbol{\Psi})}{\partial x_i}-\left(\frac{\partial\mathbf{U}}{\partial\mathbf{V}}\right)^{-\mathrm{T}}\mathbf{K}=0 \tag{27}$$

The assumption that Γ^{T} can be taken out of the spatial derivative is made and Equation (27) is, finally, expressed as

$$\frac{\partial\boldsymbol{\Psi}}{\partial t}-A_{\Gamma_i}^{\mathrm{T}}\frac{\partial\boldsymbol{\Psi}}{\partial x_i}-\left(\frac{\partial\mathbf{U}}{\partial\mathbf{V}}\right)^{-\mathrm{T}}\mathbf{K}=0 \tag{28}$$

where $\mathbf{K}$ stands for the diffusion terms

$$K_1=-\frac{T}{\varrho}\frac{\partial}{\partial x_j}\left(k\frac{\partial\Psi_{\Gamma_4}}{\partial x_j}\right),\quad K_{i+1}=\frac{\partial\tau_{ij}^{(\Psi_\Gamma)}}{\partial x_j}-\tau_{ij}\frac{\partial\Psi_{\Gamma_4}}{\partial x_j},\quad K_4=\frac{T}{p}\frac{\partial}{\partial x_j}\left(k\frac{\partial\Psi_{\Gamma_4}}{\partial x_j}\right)$$

with $i=1,2$. $\tau_{ij}^{(\Psi_\Gamma)}$ are the so-called 'adjoint stresses', given by

$$\tau_{ij}^{(\Psi_\Gamma)}=(\mu+\mu_t)\left[\left(\frac{\partial\Psi_{\Gamma_{j+1}}}{\partial x_i}+u_j\frac{\partial\Psi_{\Gamma_4}}{\partial x_i}+\frac{\partial\Psi_{\Gamma_{i+1}}}{\partial x_j}+u_i\frac{\partial\Psi_{\Gamma_4}}{\partial x_j}\right)-\frac{2}{3}\delta_{ij}\left(\frac{\partial\Psi_{\Gamma_{k+1}}}{\partial x_k}+u_k\frac{\partial\Psi_{\Gamma_4}}{\partial x_k}\right)\right]$$

The inlet–outlet boundary conditions are defined by eliminating from Equation (26) the integrals of $\delta\mathbf{U}$ at the inlet and outlet:

$$\delta\mathbf{U}^{\mathrm{T}}(A_n^{\mathrm{T}}\boldsymbol{\Psi}_\Gamma)=0 \tag{29}$$

The wall boundary conditions for the adjoint equations, Equations (27), depend on the objective function under consideration. In an inverse design problem with the objective function defined by Equation (11), the following conditions must be satisfied:

$$(p-p_{\mathrm{tar}})+\Psi_{\Gamma i+1}n_i=0 \tag{30}$$

for inviscid flows or

$$\Psi_{\Gamma i+1}=-(p-p_{\mathrm{tar}})n_i,\quad i=1,2 \tag{31}$$

for viscous flows. To prove Equations (31), one may start from Equation (25); by virtue of the solid wall condition $\tau_{ij}n_in_j=0$ (which is equivalent to $\partial V_n/\partial n=0$) or $\delta\tau_{ij}n_in_j+\tau_{ij}\delta(n_in_j)=0$ (see also [27]), the first integral on the r.h.s. of Equation (25) can be expressed as

$$-\int_{S_{\mathrm{w}}}\Psi_{\Gamma_{i+1}}\delta\tau_{ij}n_j\,\mathrm{d}S=-\int_{S_{\mathrm{w}}}\frac{\Psi_{\Gamma_{i+1}}}{n_i}[\delta\tau_{ij}n_in_j+\tau_{ij}\delta(n_in_j)]\,\mathrm{d}S+\int_{S_{\mathrm{w}}}\frac{\Psi_{\Gamma_{i+1}}}{n_i}\tau_{ij}\delta(n_in_j)\,\mathrm{d}S$$

The first integral of this equation is eliminated by imposing $\Psi_{\Gamma_2}/n_1=\Psi_{\Gamma_3}/n_2$ along the solid walls which, combined with Equation (30), leads to Equations (31). Note that this integral does not appear in Equation (26).

It is interesting to comment on Equations (30) and (31). For instance, in 2D design problems, upon convergence (i.e. when $p=p_{\mathrm{tar}}$), the inviscid flow condition becomes $\Psi_{\Gamma,2}n_1+\Psi_{\Gamma,3}n_2=0$,

DOI: 10.1002/fld

which is an equivalent no-penetration condition for the adjoint to the velocity components. Also, the viscous flow condition gives $\Psi_{\Gamma,2}=\Psi_{\Gamma,3}=0$, which stands for the equivalent no-slip condition for the adjoint variables.

Irrespective of the objective function, integrals written in terms of δT and $\delta(q_j n_j \,\mathrm{d}S)$ define the wall boundary condition for Ψ_{Γ_4} which depends on the wall temperature condition. Hence, for constant wall temperature, a zero Dirichlet condition $\Psi_{\Gamma_4}=0$ is imposed; otherwise, for adiabatic flow conditions, $\partial\Psi_{\Gamma_4}/\partial x_i n_i=0$.

The remaining terms in Equation (26) give the final expression for the variation in the augmented function

$$\begin{aligned}\delta F_{\mathrm{aug}} = \delta F_b(\delta\mathbf{b}) &+ \int_{S_\mathrm{w}} [\Psi_{\Gamma_{i+1}} p - \boldsymbol{\Psi}_\Gamma^\mathrm{T} \mathbf{f}_i^\mathrm{inv}]\delta(n_i\,\mathrm{d}S) \\ &- \int_{S_\mathrm{w}} \frac{\partial \mathbf{U}^\mathrm{T}}{\partial x_k} A_n^\mathrm{T} \boldsymbol{\Psi}_\Gamma \delta x_k \,\mathrm{d}S + \int_{S_\mathrm{w}} \boldsymbol{\Psi}_\Gamma^\mathrm{T} \frac{\partial \mathbf{f}_i^\mathrm{vis}}{\partial x_i} \delta x_k n_i \,\mathrm{d}S \\ &+ \int_{S_\mathrm{w}} \frac{\Psi_{\Gamma_{i+1}}}{n_i} \tau_{ij} \delta(n_i n_j)\,\mathrm{d}S + \int_{S_\mathrm{w}} \Psi_{\Gamma_4} q_i \delta(n_i\,\mathrm{d}S) \\ &- \int_{S_\mathrm{w}} \frac{\partial u_i}{\partial x_k} \tau_{ij}^{(\Psi_\Gamma)} \delta x_k n_j \,\mathrm{d}S - \int_{S_\mathrm{w}} \frac{\partial T}{\partial x_k} k \frac{\partial \Psi_{\Gamma_4}}{\partial x_i} \delta x_k n_i \,\mathrm{d}S \end{aligned} \tag{32}$$

where, in inverse design problems,

$$\delta F_b(\delta\mathbf{b}) = \frac{1}{2}\int_{S_\mathrm{w}} (p - p_\mathrm{tar})^2 \delta(\mathrm{d}S) \tag{33}$$

In Equation (32), variations including $n_i, n_j, \mathrm{d}S$ can be expressed as $\delta(n_i\,\mathrm{d}S)=\phi_3(\delta\mathbf{b})$ and $\delta(n_i n_j)=\phi_4(\delta\mathbf{b})$ (see Appendix). Finally, using Equation (32) with appropriate functions ϕ_1 to ϕ_4 (depending on the shape parameterization), the gradient $\delta F/\delta b_i = \delta F_{\mathrm{aug}}/\delta b_i$ can be computed and used to support gradient-based methods.

The discretization of the preconditioned adjoint equations, Equation (28) (only the inviscid part is of interest here), is carried out by integrating them over the finite volumes

$$\int_\Omega \frac{\partial \boldsymbol{\Psi}}{\partial t}\,\mathrm{d}\Omega + \int_{\partial\Omega} (-A^\mathrm{T}\Gamma^\mathrm{T}\boldsymbol{\Psi})\,\mathrm{d}\partial\Omega = 0 \tag{34}$$

The discrete form of Equation (34) becomes

$$\frac{\Omega_P}{\Delta t_P}\delta\boldsymbol{\Psi}_P + \sum_{Q\in\mathrm{nei}(P)} \boldsymbol{\Phi}_{PQ}^\Psi = 0 \tag{35}$$

where, employing a Roe-like discretization, the adjoint flux is given by

$$\boldsymbol{\Phi}_{PQ}^\Psi = \tfrac{1}{2}(-A_{\Gamma_P}^\mathrm{T}\boldsymbol{\Psi}_P - A_{\Gamma_Q}^\mathrm{T}\boldsymbol{\Psi}_Q) - \tfrac{1}{2}|\tilde{A}_{\Gamma_{PQ}}^\mathrm{T}|(\boldsymbol{\Psi}_Q - \boldsymbol{\Psi}_P) \tag{36}$$

and $A_\Gamma = \Gamma A$.

DOI: 10.1002/fld

3.3. Discrete adjoint approach

The discrete adjoint approach is based on the discrete form of the preconditioned flow equations. If $\mathbf{R}^{\Gamma}=\Gamma\mathbf{R}$ is the array of the discretized preconditioned residuals of the flow equations, according to Equations (8) and (9), the gradients of F and $\mathbf{R}^{\Gamma}$ with respect to $\mathbf{b}$ are expressed as

$$\frac{\mathrm{d}F}{\mathrm{d}\mathbf{b}}=\frac{\partial F}{\partial \mathbf{U}}\frac{\mathrm{d}\mathbf{U}}{\mathrm{d}\mathbf{b}}+\frac{\partial F}{\partial \mathbf{b}} \tag{37}$$

$$\frac{\mathrm{d}\mathbf{R}^{\Gamma}}{\mathrm{d}\mathbf{b}}=\frac{\partial \mathbf{R}^{\Gamma}}{\partial \mathbf{U}}\frac{\mathrm{d}\mathbf{U}}{\mathrm{d}\mathbf{b}}+\frac{\partial \mathbf{R}^{\Gamma}}{\partial \mathbf{b}}=0 \tag{38}$$

By using Equation (37) to eliminate $\mathrm{d}\mathbf{U}/\mathrm{d}\mathbf{b}$ from Equation (37), the derivative of F with respect to the design variables becomes

$$\frac{\mathrm{d}F}{\mathrm{d}\mathbf{b}}=\frac{\partial F}{\partial \mathbf{b}}+\mathbf{\Psi}_{\Gamma}^{\mathrm{T}}\frac{\partial \mathbf{R}}{\partial \mathbf{b}} \tag{39}$$

where the adjoint variables $\mathbf{\Psi}_{\Gamma}=\Gamma^{\mathrm{T}}\mathbf{\Psi}$ are computed through the adjoint equations

$$\left(\frac{\partial \mathbf{R}}{\partial \mathbf{U}}\right)^{\mathrm{T}}\mathbf{\Psi}_{\Gamma}+\left(\frac{\partial F}{\partial \mathbf{U}}\right)^{\mathrm{T}}=0 \tag{40}$$

In both Equations (39) and (40), the variations in the preconditioned residual vector $\mathbf{R}^{\Gamma}$ were expressed in terms of variations in $\mathbf{R}$ as $\partial\mathbf{R}^{\Gamma}/\partial\mathbf{b}=\Gamma\partial\mathbf{R}/\partial\mathbf{b}$ and $\partial\mathbf{R}^{\Gamma}/\partial\mathbf{U}=\Gamma\partial\mathbf{R}/\partial\mathbf{U}$, where the term $\mathbf{R}\partial\Gamma/\partial\mathbf{U}$ is zero since $\mathbf{R}=0$ in the steady solution.

4. RESULTS

The preconditioned continuous and discrete adjoint approaches are demonstrated on a number of selected problems concerned with the inverse design and optimization of isolated and cascade airfoils at inviscid, laminar and turbulent flows.

The parameterization of the airfoils is based on Bézier–Bernstein polynomials. Two Bézier–Bernstein curves are used separately for the pressure and suction sides of each airfoil with fixed control points at the leading and trailing points. Unstructured grids with triangular elements, generated using the advancing front technique and superimposed to structured-like layers of triangles (stretched rectangular mesh whose elements split into triangles) surrounding the airfoil, are used. The initial geometries are 'randomly' generated and the target pressure distributions for inverse designs are obtained by solving the flow equations around 'reference' airfoils ('reference' airfoils are those used to compute the target pressure distribution).

4.1. Inverse design of an isolated airfoil in inviscid flow

The first case involves the inverse design of an NACA4415 airfoil at very low Mach number flow ($M_{\infty}=0.001$) and infinite flow angle of $a_{\infty}=6^{\circ}$, using the preconditioned continuous approach. Figure 3 illustrates the initial and optimal airfoil contours together with the reference one and the corresponding pressure distributions over the solid wall.

DOI: 10.1002/fld

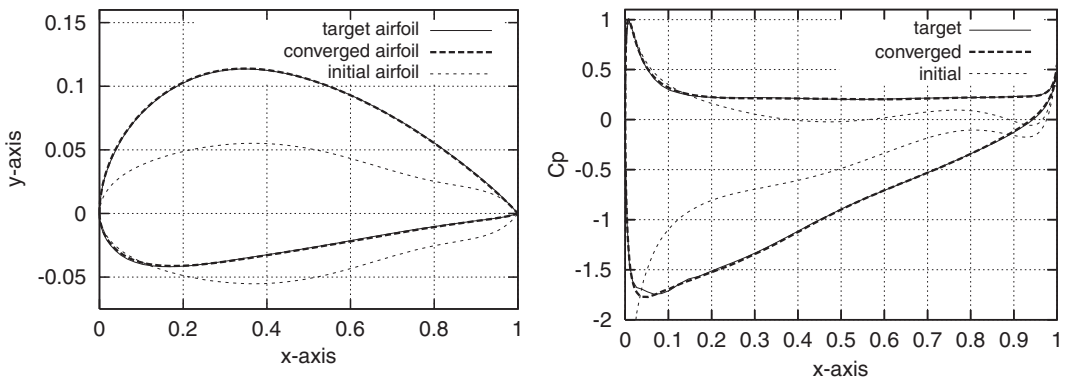

Figure 3. Inverse design of an isolated airfoil, inviscid flow. Initial, reference and optimal airfoil contours (not in scale, left) and the corresponding pressure distributions (right).

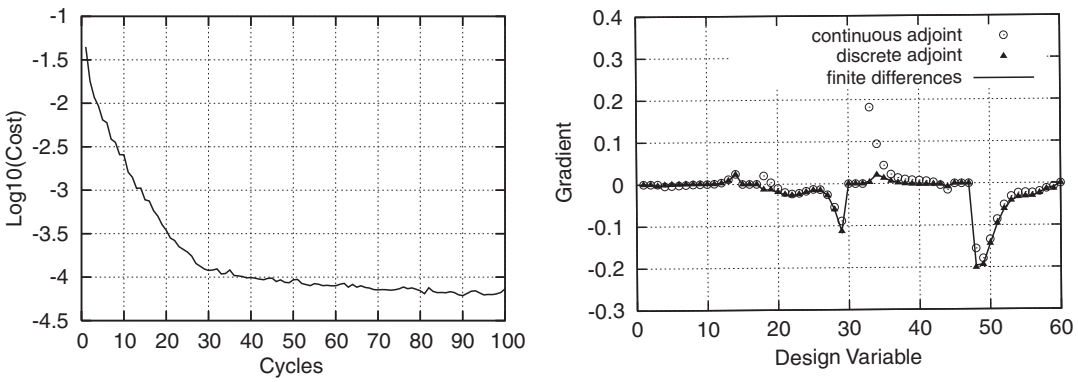

Figure 4. Inverse design of an isolated airfoil, inviscid flow. Convergence history (left) of the objective function and its gradient components for the initial airfoil computed using the preconditioned adjoint methods (continuous and discrete) and finite differences (right).

In this case, 30 control points are used. All but the leading and trailing edge control points are allowed to vary in both the chordwise and the normal-to-chord directions, summing up to 56 design variables. In Figure 4 (left), the convergence history of the optimization procedure is shown. Although other descent methods are faster, the steepest descent method was used herein since we did not focus on the reduction of the number of optimization cycles but rather on that of the CPU cost per cycle. Each optimization cycle comprises of the solution of the flow and adjoint equations. Assuming that they have almost equal CPU costs, the total required cost for convergence is approximately equal to 200 equivalent flow solutions. In the same figure (right), the objective function gradient values computed with the preconditioned continuous and discrete adjoint methods are compared with the outcome of finite differences. The first 30 design variables correspond to the chordwise (1–15) and normal-to-chord (16–30) control point coordinates of the pressure side, from the trailing to the leading edge; the next 30 variables correspond to the control points parameterizing the suction side (same sequence). The comparison is satisfactory despite

DOI: 10.1002/fld

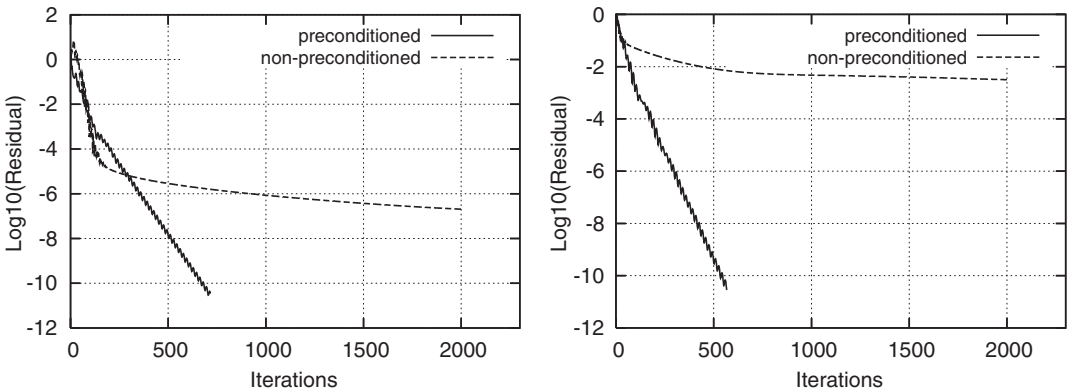

Figure 5. Inverse design of an isolated airfoil, inviscid flow. Comparison of the convergence rate of the flow (left) and adjoint (right) equations of an airfoil generated during the optimization loop with and without preconditioning.

some discrepancies of the gradient values that the continuous method produces close to the leading edge stagnation point.

The need for preconditioning both the flow and adjoint equations becomes clear in Figure 5, where the speed up of both the direct and adjoint equations is shown. Without preconditioning, the total optimization CPU cost becomes prohibitively high. Note, also, that the quality of the computed gradient values shown in Figure 4 would be damaged if the user decided to stop the runs (of both the direct and adjoint solver) prior to their convergence to machine accuracy.

4.2. Drag minimization in laminar flow

An airfoil shape optimization at laminar flow conditions is performed, targeting the minimization of the drag coefficient while maintaining a specified lift. The objective function and its variation are given by Equations (13) and (14), respectively. The free-stream Mach number is 0.01, the infinite flow angle is 3° and the Reynolds number is 500. Eight Bézier control points are used for each airfoil side. The unstructured mesh and the Mach number iso-lines of the flow field formed around the initial airfoil are shown in Figure 6 (left). The initial control points and the corresponding contour are plotted in Figure 6 (right). Note that the initial airfoil has different lift coefficient values than the target one. The weight β is set to 0.01 and the target value for the lift coefficient is $c_{l_{tar}} = 0.0861$.

In Figure 7, the initial and optimal airfoil shapes along with the corresponding pressure distributions are plotted. The convergence of the objective function value is shown in Figure 8. Figure 9 shows the objective function gradient values computed using the discrete adjoint technique in comparison with those computed using finite differences. For the purpose of a fair comparison, all solvers (direct and adjoint) were run to convergence (around eight orders of magnitude drop in residual for all equations). As shown here, the agreement between the plotted curves is satisfactory. Finally, Figure 10 shows the speed up of both the direct and adjoint equations achieved, thanks to the preconditioning. As in the previous case, if the preconditioning technique was not applied, the CPU cost of the optimization cycle increases significantly.

DOI: 10.1002/fld

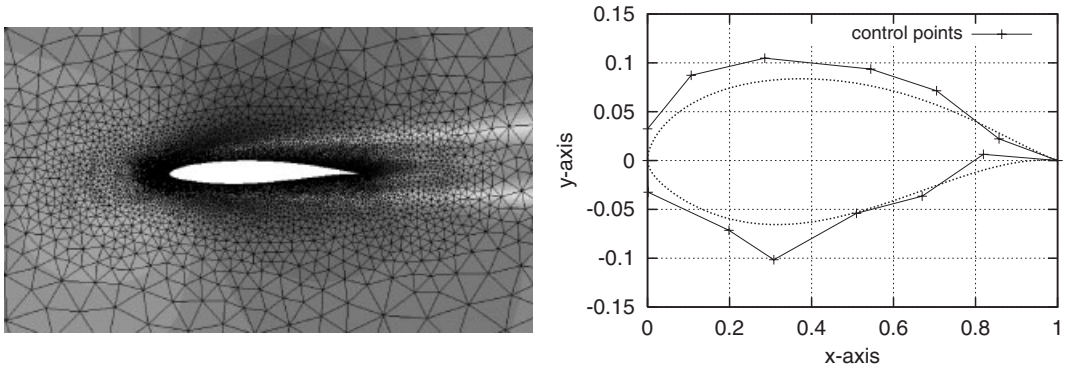

Figure 6. c_d minimization with specified c_l, laminar flow. Mesh and Mach number contours (left). Initial airfoil contour and control points (right).

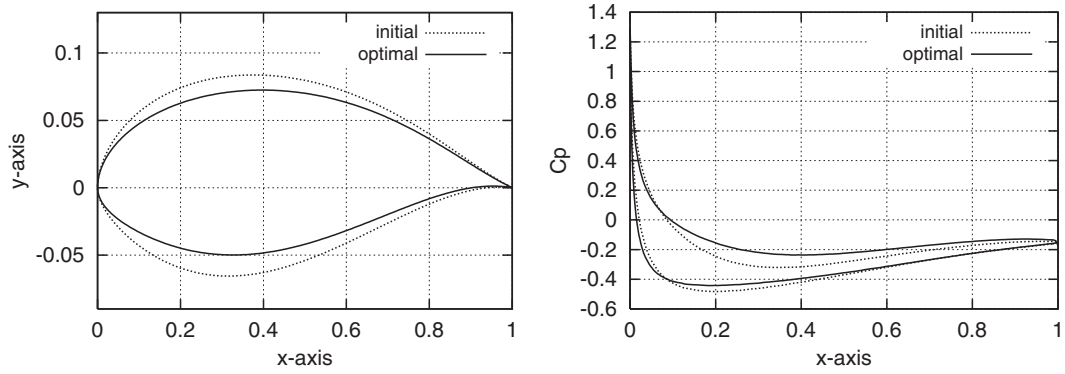

Figure 7. c_d minimization with specified c_l, laminar flow. Initial and optimal airfoil contours (not in scale, left) and the corresponding pressure distributions (right).

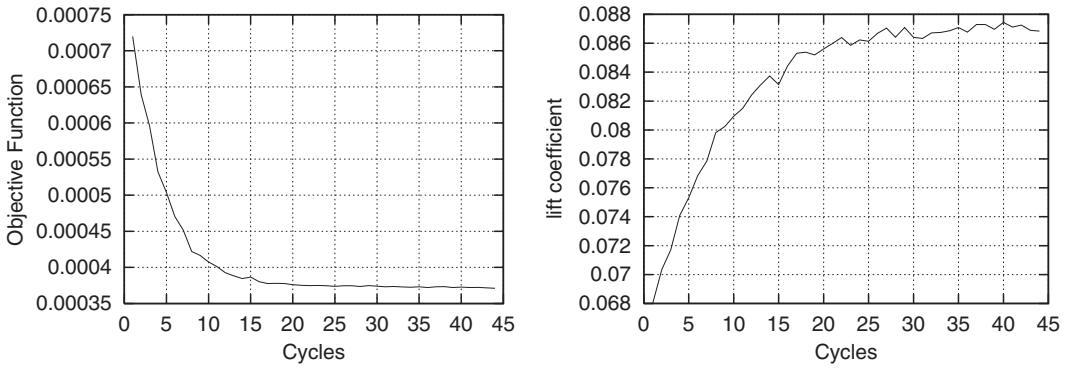

Figure 8. c_d minimization with specified c_l, laminar flow. Convergence history of the objective function (left) and the corresponding c_l values (right).

DOI: 10.1002/fld

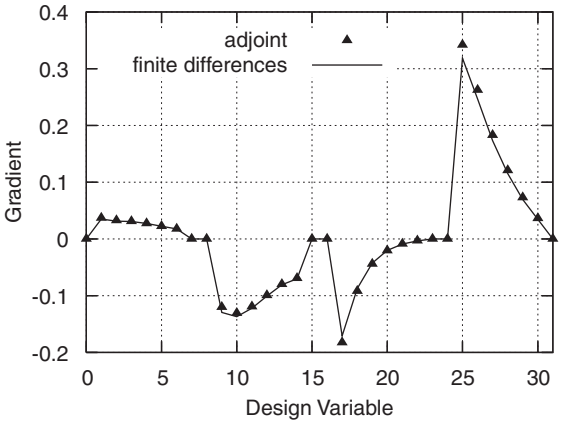

Figure 9. c_d minimization with specified c_l, laminar flow. Comparison of the gradient values computed using preconditioned discrete adjoint method and finite differences.

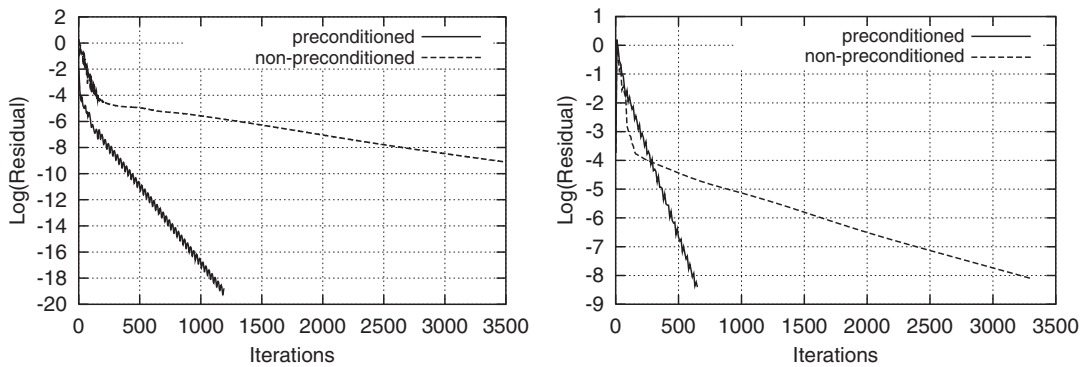

Figure 10. c_d minimization with specified c_l, laminar flow. Comparison of the convergence rate of the flow (left) and adjoint (right) equations for the initial airfoil with and without preconditioning.

4.3. Inverse design of a compressor cascade

The last case is concerned with the inverse design of a compressor cascade in turbulent flow conditions with isentropic exit Mach number $M_{2,is}=0.1$, inlet flow angle $a_1=50°$ and $Re=8\times10^5$, using the preconditioned continuous approach. The Spalart–Allmaras turbulence model [30] is used. Part of the unstructured grid near the wall region is initially formed by quadrilaterals, each of which splits into two triangles before switching to a fully unstructured grid over the rest of the domain.

The reference and optimal design with the corresponding pressure distributions are shown in Figure 11. Figure 12 presents the reduction in the value of the objective function (right) and the gradient computed with the preconditioned adjoint methods (continuous and discrete) and finite differences. Some differences are due to the fact that variations in turbulent viscosity are not taken into account during the formulation of the continuous adjoint equations. The same is valid for the

DOI: 10.1002/fld

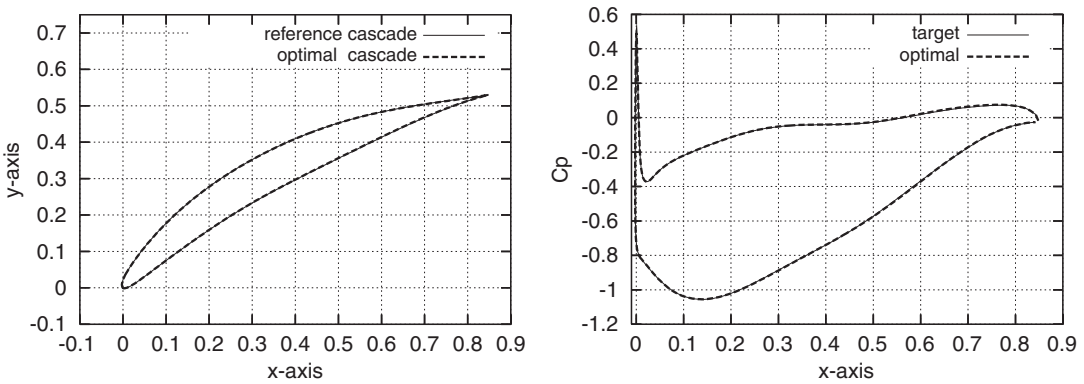

Figure 11. Inverse design of a compressor cascade, turbulent flow. Reference and optimal airfoils (left) and corresponding pressure distributions (right).

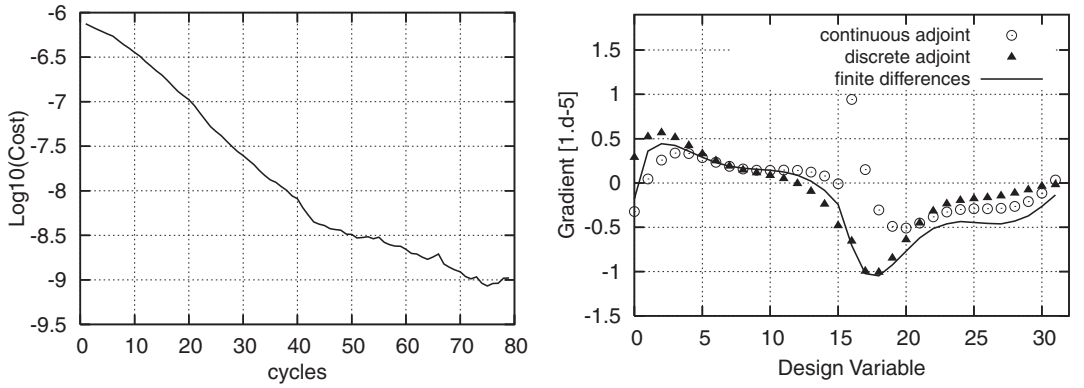

Figure 12. Inverse design of a compressor cascade, turbulent flow. Convergence history (left) and comparison of the gradient values computed using the preconditioned adjoint methods (continuous and discrete) and finite differences (right).

discrete approach, where there is no adjoint to the turbulence equation. Finally, Figure 13 compares the convergence rate for the flow and the adjoint equations with and without preconditioning. Even at a speed, which is not that low (compared with the previous cases) preconditioning speeds up the equations, and this is important for the whole optimization procedure that requires almost 80 cycles (or 160 equivalent solutions for the Navier–Stokes equations) using steepest descent.

5. CONCLUSIONS—COMMENTS

Preconditioned continuous and discrete adjoint formulations for the inverse design and optimization of isolated and cascade airfoils at low Mach number flows were presented. The proposed continuous approach relies upon an existing adjoint method for compressible flows which was adapted to

DOI: 10.1002/fld

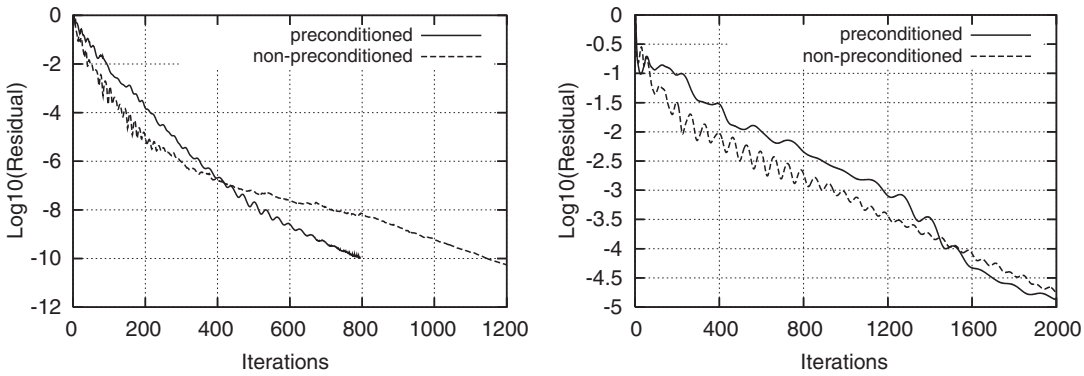

Figure 13. Inverse design of a compressor cascade, turbulent flow. Comparison of the convergence rate of the flow (left) and adjoint (right) equations for a cascade during optimization (cycle 46), with and without preconditioning.

take into account the preconditioned Navier–Stokes equations. The proposed formulations for continuous and discrete adjoints allow the inverse design and optimization of aerodynamic shapes at very low Mach numbers with reasonable CPU cost. Otherwise, standard (without preconditioning) compressible flow solvers and their adjoints become very costly or even fail to converge and so does the optimization loop as a whole.

Given the advantages of the proposed formulations, it is important to comment on the two possibilities to incorporate the preconditioner in the adjoint methods. There are two alternatives, which are: (a) to set up the adjoint to the preconditioned flow equations as we did in this paper and (b) to precondition the adjoint equations derived from the non-preconditioned flow equations. Under certain assumptions, these can be proved to be equivalent. The preceding analysis of Section 3.2, started from the preconditioned flow equations $\partial\mathbf{U}/\partial t+\Gamma A_i\partial\mathbf{U}/\partial x_i=0$ (for the sake of simplicity, we use the Euler equations) and concluded to the adjoint to the preconditioned equations, namely

$$\frac{\partial\mathbf{\Psi}}{\partial t}-A_i^{\mathrm{T}}\Gamma^{\mathrm{T}}\frac{\partial\mathbf{\Psi}}{\partial x_i}=0 \tag{41}$$

Another possibility would be to apply the preconditioner after obtaining the adjoint to the non-preconditioned flow equations (i.e. $\partial\mathbf{\Psi}/\partial t-A_i^{\mathrm{T}}\partial\mathbf{\Psi}/\partial x_i=0$). To do so, the time derivative of the adjoint equations must be multiplied by the inverse transpose of an appropriate preconditioner $\mathscr{D}$, leading to

$$\frac{\partial\mathbf{\Psi}}{\partial t}-\mathscr{D}^{\mathrm{T}}A_i^{\mathrm{T}}\frac{\partial\mathbf{\Psi}}{\partial x_i}=0 \tag{42}$$

The last expression becomes identical to Equation (41) if we choose $A\mathscr{D}=\Gamma A$. This is not an arbitrary choice, because it assures that arrays $A\mathscr{D}$ and ΓA have the same eigenvalues, thus giving rise to better convergence characteristics for both the flow and adjoint equations.

DOI: 10.1002/fld

APPENDIX A: SHAPE PARAMETERIZATION

The variations in the finite arc length $\mathrm{d}S$, the dimensional normal vector components $n_i\,\mathrm{d}S$ or the grid coordinates x_j over the airfoil are computed using the adopted parameterization scheme which is, herein, based on Bézier–Bernstein polynomials [31]. The x_j coordinates along the shape contour are given by the expression

$$x_j(t)=\sum_{i=0}^{M-1} C_i(t)X_{ij} \tag{A1}$$

where $j=1,2$ in 2D, M is the number of control points ($i=1,\ldots,M$), $C_i(t)$ are the Bézier–Bernstein polynomials and X_{ij} are the control point coordinates. The variation in x_j with respect to X_{ij} is directly computed as

$$\delta x_j=\sum_{i=0}^{M-1} C_i(t)\delta X_{ij} \tag{A2}$$

The finite length $\mathrm{d}S$ is given by

$$(\mathrm{d}S)^2=(\mathrm{d}t)^2\left(\sum_{i=0}^{M-1}\dot{C}_i(t)X_{ij}\right)^2 \tag{A3}$$

where $\dot{C}_i(t)=(\mathrm{d}C_i/\mathrm{d}t)(t)$. Its variation with respect to the variation in the control points is given by

$$\delta(\mathrm{d}S)=\frac{(\mathrm{d}t)^2}{\mathrm{d}S}\dot{x}_j\left(\sum_{i=0}^{M-1}\dot{C}_i(t)\delta X_{ij}\right) \tag{A4}$$

in which $\dot{x}_i=\mathrm{d}x_i/\mathrm{d}t=\sum_{i=0}^{M-1}\dot{C}_i(t)X_{ij}$. Since, in a 2D case,

$$\mathbf{n}=(n_1,n_2)=\left(-\frac{\mathrm{d}x_2}{\mathrm{d}S},\frac{\mathrm{d}x_1}{\mathrm{d}S}\right) \tag{A5}$$

the variations in n_1 and n_2 are given by

$$\begin{aligned}
\delta n_1&=-\frac{\mathrm{d}t}{\mathrm{d}S}\left((1-n_1^2)\sum_{i=0}^{M-1}\dot{C}_i(t)\delta X_{i2}+n_1n_2\sum_{i=0}^{M-1}\dot{C}_i(t)\delta X_{i1}\right)\\
\delta n_2&=\frac{\mathrm{d}t}{\mathrm{d}S}\left((1-n_2^2)\sum_{i=0}^{M-1}\dot{C}_i(t)\delta X_{i1}+n_1n_2\sum_{i=0}^{M-1}\dot{C}_i(t)\delta X_{i2}\right)
\end{aligned} \tag{A6}$$

Variations in $n_i\,\mathrm{d}S$ can be derived from Equations (A4) and (A6), in a straightforward manner, i.e. $\delta(n_i\,\mathrm{d}S)=\delta(n_i)\,\mathrm{d}S+n_i\delta(\mathrm{d}S)$

ACKNOWLEDGEMENTS

This work is funded by the NTUA Basic Research Program 'Lefkippos'. The second author is supported by a grant from the State Scholarships Foundation of Greece.

DOI: 10.1002/fld

REFERENCES

1. Anderson WK, Newman JC, Whitfield DL, Nielsen EJ. Sensitivity analysis for the Navier–Stokes equations on unstructured meshes using complex variables. *Fourteenth AIAA Computational Fluid Dynamics Conference*, Norfolk, VA, AIAA Paper 1999-3294, June 1999.
2. Nadarajah S, Jameson A. A comparison of the continuous and discrete adjoint approach to automatic aerodynamic optimization. *Thirty-eighth AIAA Aerospace Sciences Meeting and Exhibit*, Reno, NV, AIAA Paper 2000-0667, January 2000.
3. Pironneau O. *Optimal Shape Design for Elliptic Systems*. Springer: New York, 1984.
4. Jameson A. Aerodynamic design via control theory. *Journal of Scientific Computing* 1998; **3**:233–260.
5. Jameson A. Optimum aerodynamic design using CFD and control theory. *Twelfth AIAA Computational Fluid Dynamics Conference*, San Diego, CA, AIAA Paper 1995-1729, June 1995.
6. Jameson A, Pierce N, Martinelli L. Optimum aerodynamic design using the Navier–Stokes equations. *Theoretical and Computational Fluid Dynamics* 1998; **10**:213–237.
7. Anderson WK, Venkatakrishnan V. Aerodynamic design optimization on unstructured grids with a continuous adjoint formulation. *Thirty-fifth AIAA Aerospace Sciences Meeting and Exhibit*, Reno, NV, AIAA Paper 1997-0643, January 1997.
8. Pierce NA, Giles MB. An introduction to the adjoint approach to design. *Flow*, *Turbulence and Combustion* 2000; **65**:393–415.
9. Nielsen EJ, Lu J, Park MA, Darmofal DL. An implicit, exact dual adjoint solution method for turbulent flows on unstructured grids. *Computers and Fluids* 2004; **33**:1131–1155.
10. Reuther J, Rimlinger MJ, Alonso JJ, Jameson A. Aerodynamic shape optimization of supersonic aircraft configurations via an adjoint formulation on distributed memory parallel computers. *Sixth AIAA/USAF/NASA/ISSMO Symposium on Multidisciplinary Analysis and Optimization*, Bellevue, WA, AIAA Paper 1996-4045, September 1996.
11. Jameson A, Shankaran S, Martinelli L, Haimes B. Aerodynamic shape optimization of complete aircraft configuration. *Forty-second AIAA Aerospace Sciences Meeting and Exhibit*, Reno, NV, AIAA Paper 2004-0533, January 2004.
12. Kim H, Sasaki D, Obayashi S, Nakahashi K. Aerodynamic optimization of supersonic transport wing using unstructured adjoint method. *AIAA Journal* 2001; **39**:1011–1020.
13. Anderson WK, Bonhaus DL. Airfoil design on unstructured grids for turbulent flows. *AIAA Journal* 1999; **37**:185–191.
14. Giles MB. Discrete adjoint approximations with shocks. *Hyperbolic Problems*: *Theory*, *Numerics*, *Applications*. Springer: Berlin, 2003.
15. Harbeck M, Jameson A. Exploring the limits of transonic shock-free airfoil design. *Forty-third AIAA Aerospace Sciences Meeting and Exhibit*, Reno, NV, AIAA Paper 2005-1041, January 2005.
16. Papadimitriou D, Giannakoglou K. Compressor blade optimization using a continuous adjoint formulation. *ASME Gas Turbine & Aeroengine Technical Congress and Exposition*, Barcelona, Spain, ASME Paper GT2006-90466, May 2006.
17. Nadarajah S, McMullen M, Jameson A. Non-linear frequency domain based optimum shape design for unsteady three-dimensional flow. *Forty-fourth AIAA Aerospace Sciences Meeting and Exhibit*, Reno, NV, AIAA Paper 2006-1052, January 2006.
18. Thomas JP, Hall KC, Dowell EH. A discrete adjoint approach for modeling unsteady aerodynamic design sensitivities. *Forty-first AIAA Aerospace Sciences Meeting and Exhibit*, Reno, NV, AIAA Paper 2003-0041, January 2003.
19. Kuruvila G, Taasan S, Salas MD. Airfoil design and optimization by the one-shot method. *Thirty-third AIAA Aerospace Sciences Meeting and Exhibit*, Reno, NV, AIAA Paper 1995-478, January 1995.
20. Hazra S, Schulz V, Brezillon J, Gauger N. Aerodynamic shape optimization using simultaneous pseudo-timestepping. *Journal of Computational Physics* 2005; **204**:46–64.
21. Dadone A, Grossman B. Fast convergence of inviscid fluid dynamic design problems. *Computers and Fluids* 2003; **32**:607–627.
22. Mohammadi B, Pironneau O. Shape optimization in fluid mechanics. *Annual Review of Fluid Mechanics* 2004; **36**:255–279.
23. Soto O, Lohner R. On the computation of flow sensitivities from boundary integrals. *Forty-second AIAA Aerospace Sciences Meeting and Exhibit*, Reno, NV, AIAA Paper 2004-0112, January 2004.

DOI: 10.1002/fld

24. Turkel E. Preconditioned methods for solving the incompressible and low speed compressible equations. *Journal of Computational Physics* 1987; **72**:277–298.
25. Eriksson LE. A preconditioned Navier–Stokes solver for low mach number flows. *Third ECCOMAS CFD Conference*, Paris, September 1996.
26. Choi YH, Merkle CL. The application of preconditioning in viscous flows. *Journal of Computational Physics* 1993; **105**:207–233.
27. Papadimitriou D, Giannakoglou K. A continuous adjoint method with objective function derivatives based on boundary integrals for inviscid and viscous flows. *Computers and Fluids* 2007; **36**:325–341.
28. Roe PL. Approximate Riemann solvers, parameter vectors, and difference schemes. *Journal of Computational Physics* 1981; **43**:357–372.
29. van Leer B, Lee WT, Roe PL. Characteristic time-stepping or local preconditioning of the Euler equations. *Tenth AIAA Computational Fluid Dynamics Conference*, Honolulu, HI, AIAA Paper 1991-1552, June 1991.
30. Spalart P, Allmaras S. A one-equation turbulence model for aerodynamic flows. *La Recherche Aerospatiale* 1994; **1**:5–21.
31. Forest AR. Interactive interpolation and approximation by Bézier polynomials. *The Computer Journal* 1972; **15**:71–79.

DOI: 10.1002/fld